crystals

MDPI

Article

Conductive Supramolecular Architecture Constructed from Polyoxovanadate Cluster and Heterocyclic Surfactant

Toshiyuki Misawa, Minako Taira, Katsuhiko Fujio and Takeru Ito *

Department of Chemistry, School of Science, Tokai University, 4-1-1 Kitakaname, Hiratsuka 259-1292, Japan; t.misawa3303@gmail.com (T.M.); m.n.k.881018@gmail.com (M.T.); kfujio@tokai-u.jp (K.F.)

* Correspondence: takeito@keyaki.cc.u-tokai.ac.jp; Tel.: +81-463-58-1211 (ext. 3737)

Received: 30 December 2017; Accepted: 22 January 2018; Published: 25 January 2018

Abstract: Proton-conductive solid electrolytes are significant for fuel-cell battery technology. Especially for use in motor vehicles, proton conductors which work at intermediate temperatures (373–673 K) under an anhydrous atmosphere are desired to improve the fuel cell stability and efficiency. Inorganic–organic hybrid supramolecular architectures are a promising option for the realization of highly conductive proton conductors. Here, a hybrid layered crystal was synthesized for the first time by using an proton-containing decavanadate (V_{10}) anion and a heterocyclic surfactant cation. A simple ion-exchange reaction led to the formation of an inorganic–organic hybrid of V_{10} by using dodecylpyridazinium (C_{12}pda) as the heterocyclic surfactant. Single crystal X-ray analyses revealed that four C_{12}pda cations were associated with one V_{10} anion, which was a diprotonated species forming a one-dimensional infinite chain structure through hydrogen bonds. Anhydrous proton conductivity was investigated by alternating current (AC) impedance spectroscopy in the range of 313–393 K, exhibiting a maximum value of 1.7×10^{-5} S cm^{-1} at 373 K.

Keywords: inorganic–organic; hybrid crystal; polyoxometalate; heterocyclic; surfactant; proton conductivity

1. Introduction

Supramolecular chemistry enables the production of a variety of self-organized architectures from the artificial to the biological [1], which include static and dynamic systems [2]. In addition, supramolecular chemistry can produce inorganic–organic hybrid materials which exhibit characteristic functions derived from the synergy of inorganic and organic components [3–5]. Recently, toward the application to fuel-cell batteries [6], crystalline inorganic–organic hybrids such as MOFs (metal–organic frameworks) or PCPs (porous coordination polymers) have been widely investigated as a possible substitution for the present polymer proton conductors [7–12].

As for inorganic components, polyoxometalate (POM) clusters are promising due to their unique redox properties [13–19]. Heteropolyacids, Keggin-type POMs with a proton as counter cation, have been investigated as high proton conductors [20–26]. Such POMs have been successfully hybridized by surfactant cations to form inorganic–organic hybrids [27–35] and single crystals [36–55]. These polyoxometalate–surfactant hybrids allow various combinations of the ionic components, leading to precise engineering of the structure and function.

Among several POMs, a polyoxovanadate such as decavanadate ($[V_{10}O_{28}]^{6-}$, V_{10}, Figure 1), tends to be associated with protons [56–61]. Therefore, polyoxovanadate–surfactant hybrid crystals are promising as proton-conducting materials, and anhydrous proton conductivity has been evaluated for the V_{10} hybrid crystals comprising decyltrimethylammonium ($[(C_{10}H_{21})N(CH_3)_3]^+$, C_{10}) surfactant [47]. The anhydrous proton conductivity could be enhanced by the delocalized π–electrons

in the heterocyclic moiety of the hybridized surfactant. However, no V_{10} hybrid crystal comprising the surfactant with a heterocyclic moiety has been reported.

Here we demonstrate the first syntheses and structural analyses of V_{10}-heterocyclic surfactant hybrid crystals. Dodecylpyridazinium ($[C_4H_4N_2(C_{12}H_{25})]^+$ (C_{12}pda), Figure 1) cation was employed as the heterocyclic surfactant. The C_{12}pda cation has been rarely reported to form hybrid crystals with POMs [44]. In the crystal structure, the V_{10} anion formed a diprotonated species, and anhydrous proton conductivity was elucidated.

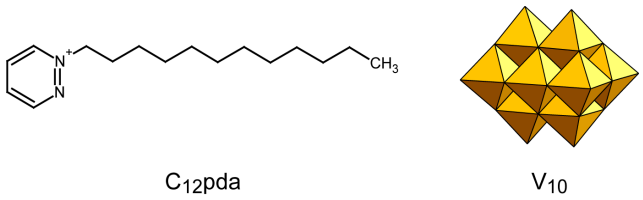

Figure 1. Molecular structures of dodecylpyridazinium (C_{12}pda) cation (**left**) and decavanadate (V_{10}) anion (**right**).

2. Materials and Methods

2.1. Materials and Genaral Methods

All chemical reagents were purchased from Wako Pure Chemical Industries, Ltd. (Wako, Osaka, Japan) and Tokyo Chemical Industry Co., Ltd. (TCI, Tokyo, Japan). $[C_4H_4N_2(C_{12}H_{25})]$Br ($C_{12}$pda·Br) was synthesized by using pyridazine and 1-bromododecane based on the literature [62].

Infrared (IR) spectra (as KBr pellet) were recorded on a Jasco FT/IR-4200ST spectrometer (JASCO Corporation, Tokyo, Japan). Powder X-ray diffraction (XRD) patterns were measured with a Rigaku MiniFlex300 diffractometer (Rigaku Corporation, Tokyo, Japan) by using Cu Kα radiation (λ = 1.54056 Å) at ambient temperature. Diffuse reflectance ultraviolet-visible (UV-vis) spectra were collected with a Jasco V-670 spectrometer (JASCO Corporation, Tokyo, Japan).

Conductivity measurements were carried out by alternating current (AC) impedance method in a frequency range from 20 to 1.0 $\times$ 10^7 Hz using a Wayne Kerr 6510P inductance-capacitance-resistance (LCR) meter. Pelletized powder samples (10 mm in diameter, 0.81 mm in thickness) were sandwiched with Pt electrodes, and the impedance was measured under a dry N_2 atmosphere at 313–393 K.

2.2. Synthesis

C_{12}pda-V_{10} hybrids were synthesized as follows: solid V_2O_5 (0.40 g, 2.2 mmol) was dispersed in 15 mL of water, and dissolved by adding LiOH·H_2O (0.24 g, 5.7 mmol). The solution was adjusted to pH 6.0 or 4.0 with 6M HCl, and the resulting orange solution was added at room temperature to an ethanol solution (15 mL) of C_{12}pda·Br (0.30 g, 0.91 mmol) with stirring for 60 min. Obtained dark green (pH 6.0) or yellow (pH 4.0) precipitates were filtered off, and washed with 10 mL of ethanol to obtain as-prepared product of C_{12}pda-V_{10} (0.377 g (56% yield) for pH 6.0; 0.179 g (34% yield) for pH 4.0).

Yellow plate crystals suitable for X-ray diffraction measurements were obtained from the filtrate of the synthesis at pH 6.0 kept at 279 K for 4–5 months. The yellow plate crystals were also obtained from the filtrate of the synthesis at pH 4.0 kept at 293 K for two weeks. Anal.: Calcd for $C_{66}H_{126}N_8V_{10}O_{30}$: C: 39.22, H: 6.28, N: 5.54%. Found: C: 38.22, H: 6.18, N: 5.48%. IR (KBr disk): 959 (s), 827 (m), 755 (m), 721 (m), 607 (m), 446 (w), 407 (w) cm^{-1}.

2.3. X-ray Crystallography

Single crystal X-ray diffraction data for the C_{12}pda-V_{10} crystals were recorded with an ADSC Q210 CCD area detector with a synchrotron radiation at the 2D beamline in Pohang Accelerator

Laboratory (PAL). The diffraction images were processed by using HKL3000 [63], and absorption correction was also performed with HKL3000. The structure was solved by the direct method using SHELXT Version 2014/5 [64] and refined by the full-matrix least-squares method on F^2 using SHELXL Version 2014/7 [65]. All calculations were performed using the CrystalStructure software package [66]. All non-hydrogen atoms were refined anisotropically. The H atoms attached to the O atoms of V_{10} were found in the difference Fourier synthesis and their positional and isotropic displacement parameters were refined. The hydrogen atoms of C_{12}pda surfactants and ethanol molecule of crystallization were refined using the riding model. Further details of the crystal structure investigation may be obtained free of charge from the Cambridge Crystallographic Data Centre, 12 Union Road, Cambridge CB2 1EZ, UK; fax: (+44) 1223 336 033; or E-Mail: deposit@ccdc.cam.ac.uk (CCDC 1813634).

3. Results

3.1. Syntheses of C_{12}pda-V_{10} hybrids

C_{12}pda-V_{10} hybrids were obtained as insoluble precipitates from aqueous solution of solid V_2O_5, the pH of which was adjusted at 6.0 or 4.0. The C_{12}pda-V_{10} hybrids synthesized at pH 6.0 were dark green, while the C_{12}pda-V_{10} hybrids synthesized at pH 4.0 were yellow. In this pH range, the V_{10} anions or their protonated species are the main species in the solution [67]. Figure 2a,b shows Infrared (IR) spectra of these dark green and yellow C_{12}pda-V_{10} hybrids, in which the characteristic peaks for the V_{10} anion were observed in the range of 400–1000 cm^{-1}. This means that both C_{12}pda-V_{10} hybrids synthesized at pH 6.0 and 4.0 contained the V_{10} anion, although the sample colors were different (dark green and yellow). The dark green color will be derived from the reduced V_{10} species. On the other hand, the C_{12}pda-V_{10} hybrids synthesized at pH 6.0 and 4.0 exhibited different powder X-ray diffraction (XRD) patterns (Figure 3a,b), indicating that these hybrids had different bulk structures.

The yellow-colored C_{12}pda-V_{10} crystals were obtained from the synthetic filtrate at pH 6.0. The C_{12}pda-V_{10} crystals were identified to possess the same molecular and crystal structure as the yellow C_{12}pda-V_{10} hybrids synthesized at pH 4.0, which was revealed by the IR spectrum (Figure 2b,c) and powder XRD pattern (Figure 3b,c). The yellow crystalline hybrids were employed for the conductivity measurements (see below). The XRD pattern of the C_{12}pda-V_{10} crystals was different in peak positions from that calculated from the results of single crystal X-ray analyses (Figure 3d). This may be due to the difference in the measurement temperature (powder: ambient temperature, single crystal: 100 K) and the desolvation of solvent molecules of the crystals during the XRD measurements.

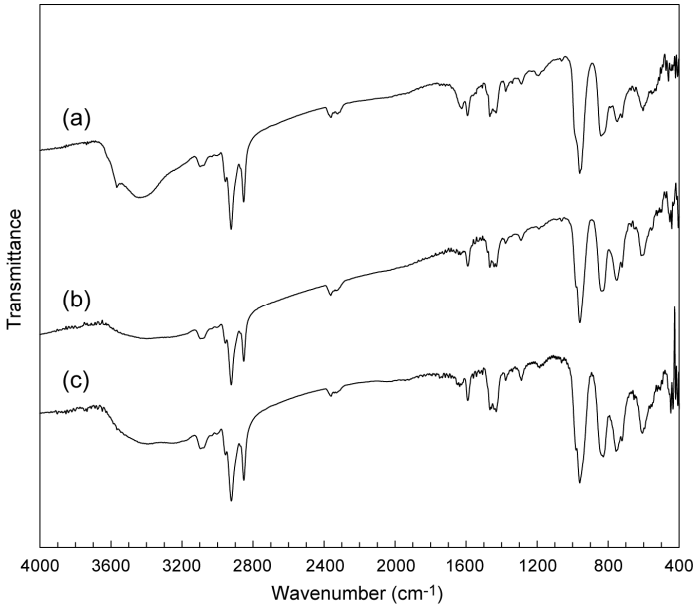

Figure 2. IR spectra of C_{12}pda-V_{10} hybrids: (**a**) dark green C_{12}pda-V_{10} hybrids synthesized at pH 6.0; (**b**) yellow C_{12}pda-V_{10} hybrids synthesized at pH 4.0; (**c**) C_{12}pda-V_{10} crystals obtained from the filtrate of the synthesis at pH 6.0.

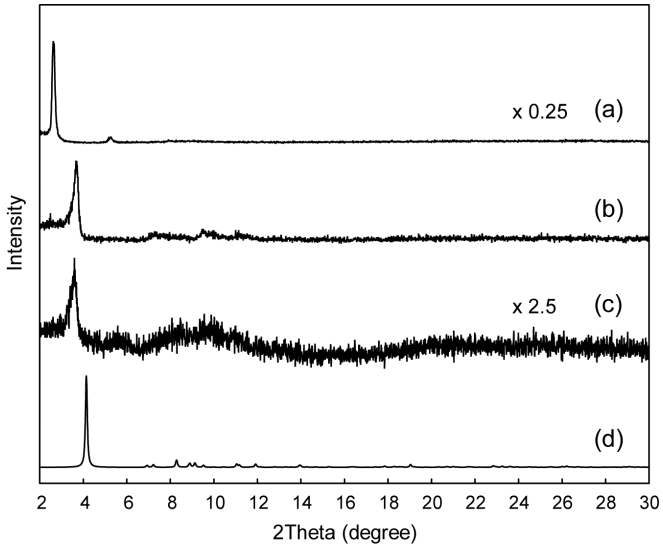

Figure 3. Powder X-ray diffraction patterns of C_{12}pda-V_{10} hybrids: (**a**) dark green C_{12}pda-V_{10} hybrids synthesized at pH 6.0; (**b**) yellow C_{12}pda-V_{10} hybrids synthesized at pH 4.0; (**c**) C_{12}pda-V_{10} crystals obtained from the filtrate of the synthesis at pH 6.0; (**d**) Calculated pattern of C_{12}pda-V_{10} crystals using the structure obtained by single-crystal X-ray diffraction.

3.2. Crystal Structure of C_{12}pda-V_{10}

The X-ray structure and elemental analyses revealed the formula of the C_{12}pda-V_{10} crystals to be $[C_4H_4N_2(C_{12}H_{25})]_4[H_2V_{10}O_{28}]\cdot H_2O\cdot C_2H_5OH$ (Table 1, Figure 4). The crystal consisted of the V_{10} anion, being consistent with the IR spectrum (Figure 2c). Four C_{12}pda cations (1+ charge) were associated with one V_{10} anion (6- charge) due to the charge compensation, suggesting the presence of two protons as counter cation in the C_{12}pda-V_{10} crystals. The protons were connected to the V_{10}

anion to form $[H_2V_{10}O_{28}]^{4-}$ (H_2V_{10}) as observed in the hybrid crystals of the V_{10} anion and C_{10} cation (C_{10}-V_{10}) [47] (see below).

The crystal packing of C_{12}pda-V_{10} was composed of alternating V_{10} inorganic monolayers and C_{12}pda organic bilayers parallel to the *bc* plane with an interlayer distance of 25.5 Å (Figure 4a). The dodecyl chains of C_{12}pda were interdigitated straightly with each other. The solvent molecules (water and ethanol) of crystallization were placed at the interface between the V_{10} and C_{12}pda layers (Figure 4a).

The V_{10} anion in the C_{12}pda-V_{10} crystals was clearly identified as a diprotonated species by the X-ray structure analyses (Figure 4b). This result was confirmed by the bond valence sum (BVS) calculations [68] giving values of 1.37 (O15) and 1.24 (O24), while the BVS values were within the range 1.63–2.03 for other oxygen atoms. Each diprotonated V_{10} anion was related by the two-fold screw axis, and connected by the O–H···O hydrogen bond to form a one-dimensional infinite chain structure (Figure 4c). The O···O distances were 2.740(2) Å for O15–H66···O17^i (symmetry code *i*: $1 - x$, $-0.5 + y$, $0.5 - z$) and 2.766(2) Å for O24–H67···O9^i, respectively. The C_{12}pda-V_{10} crystals had a zigzag infinite chain structure of V_{10} different from the chain structure observed in the C_{10}-V_{10} crystals [47], which would be caused by the different manner of the protonation. In the C_{12}pda-V_{10} crystals, one protonated oxygen site (O15) was different from the case of the C_{10}-V_{10} hybrid crystals, resulting in a different arrangement of the V_{10} anions from that in the C_{10}-V_{10} crystals. These hydrogen-bonded V_{10} chains were formed in the inorganic layers, and isolated by the pyridazinium moieties of the C_{12}pda cations.

Table 1. Crystallographic data of C_{12}pda-V_{10} crystal.

Compound	**C_{12}pda-V_{10}**
Chemical formula	$C_{66}H_{124}N_8V_{10}O_{30}$
Formula weight	2019.16
Crystal system	Monoclinic
Space group	$P2_1/c$ (No. 14)
a (Å)	26.183(2)
b (Å)	15.828(2)
c (Å)	21.891(2)
α (°)	90.0000
β (°)	103.094(2)
γ (°)	90.0000
V (Å^3)	8836.3(15)
Z	4
ρ_{calcd} (g cm^{-3})	1.518
T (K)	100(2)
Wavelength (Å)	0.63000
μ (mm^{-1})	1.045
No. of reflections measured	249,472
No. of independent reflections	35,308
R_{int}	0.0740
No. of parameters	1041
R_1 ($I > 2\sigma(I)$)	0.0565
wR_2 (all data)	0.1652

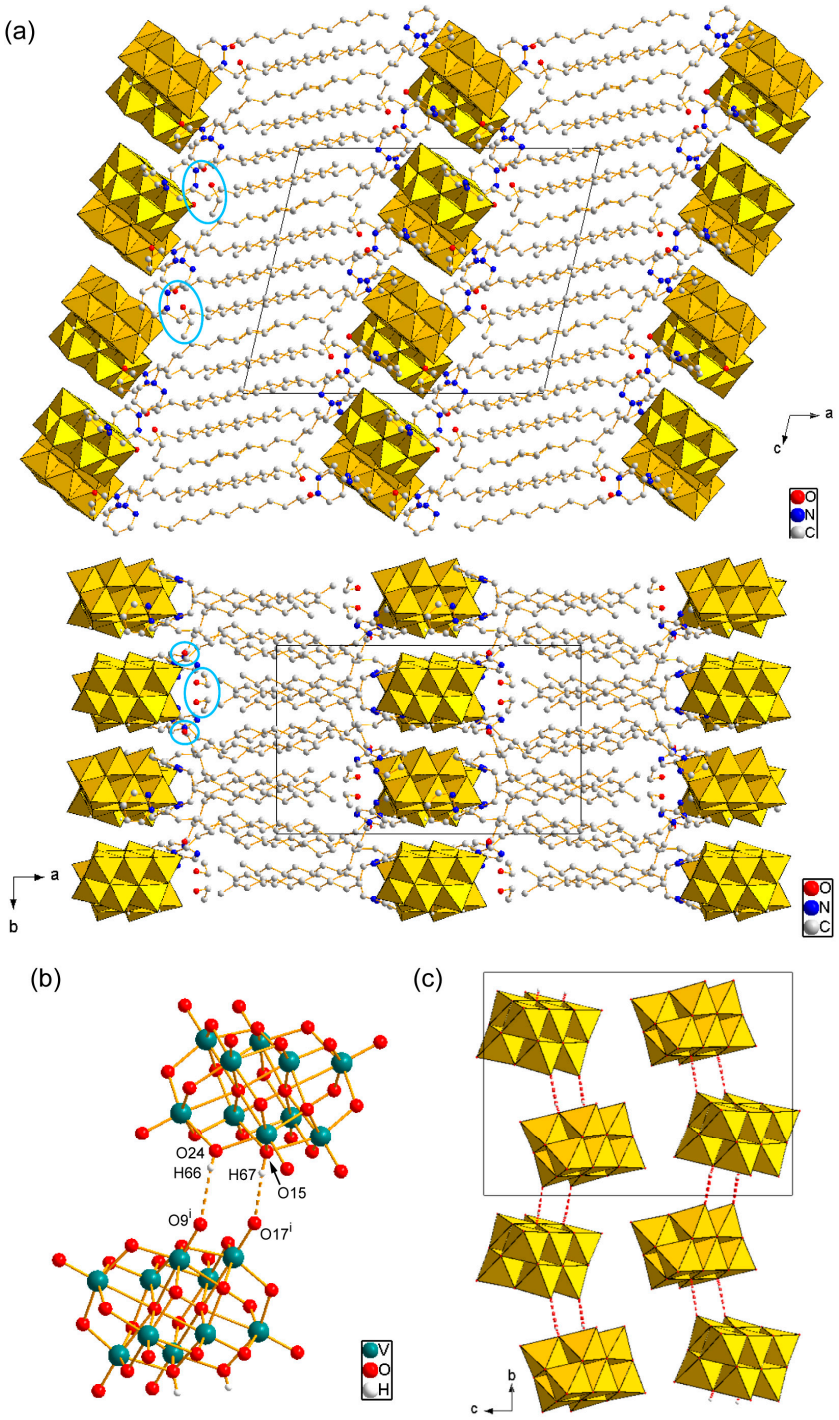

Figure 4. Crystal structure of C_{12}pda-V_{10} (C: gray, N: blue, O: red, H: white); (**a**) packing diagram along *b* axis (upper) and *c* axis (lower). V_{10} anions in polyhedral representation. H atoms of C_{12}pda and ethanol of crystallization are omitted for clarity. Some solvent molecules are highlighted; (**b**) molecular structure of diprotonated V_{10} anion. Another V_{10} anion is generated by the symmetry operation $(1 - x, -0.5 + y, 0.5 - z)$. Symmetry code: (i) $1 - x, -0.5 + y, 0.5 - z$; (**c**) molecular arrangements in the inorganic layers. V_{10} anions in polyhedral representation. The short contacts derived from O-H···O hydrogen bonds are represented in red broken lines. The C_{12}pda cations and solvents of crystallization are omitted for clarity.

The structural features of the C_{12}pda cations were then investigated. Although most C–C bonds of the dodecyl chains of C_{12}pda had an *anti* conformation, three C–C bonds (C22–C23, C40–C41, C56–C57) had a *gauche* conformation (Figure 5a), two of which (C40–C41, C56–C57) were located some methylene groups away from the hydrophilic head, which was similar to the C_{12}pda conformation in the hybrid crystal comprising decatungstate ($[W_{10}O_{32}]^{4-}$, W_{10}) anion (C_{12}pda-W_{10}) [44]. The hydrophilic heads of C_{12}pda penetrated into the V_{10} inorganic layers as mentioned above. The penetrated pyridazine rings of C_{12}pda had short contacts between the heterocyclic moiety due to the C–H···π interactions (Figure 5b), being different from the C_{12}pda-W_{10} hybrid crystal [44]. The C_{12}pda cation interacted with the V_{10} anions by C–H···O hydrogen bonds [69] with C···O distances ranging from 2.82 to 3.92 Å (mean value: 3.33 Å), most of which were formed between the V_{10} anion and pyridazine rings of the C_{12}pda cations.

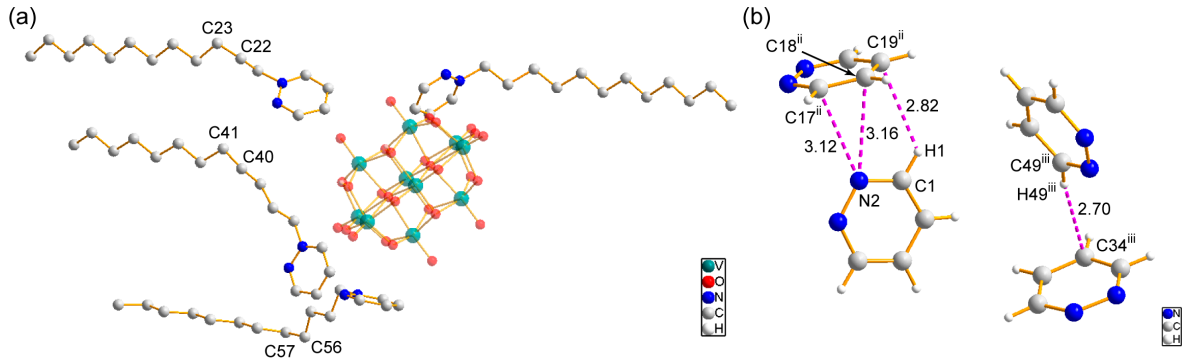

Figure 5. View of crystallographically-independent surfactant molecules; (**a**) whole C_{12}pda cations in the asymmetric unit together with V_{10} anion; (**b**) pyridazinium moieties of the C_{12}pda cations in the vicinity of the V_{10} anions. The distances of short contacts are represented in Å unit. Symmetry code: (*ii*) $1-x, 1-y, 1-z$; (*iii*) $x, 1.5-y, 0.5+z$.

3.3. Anhydrous Proton Conductivity of C_{12}pda-V_{10}

The anhydrous proton conductivity was investigated for the yellow C_{12}pda-V_{10} hybrids by alternating current (AC) impedance spectroscopy. Figure 6a shows a typical Nyquist spectrum, which was measured at 373 K under a dry N_2 atmosphere. The spectrum showed a suppressed half circle in the high- and medium-frequency regions and a slightly inclined line in the low-frequency region. The Nyquist spectrum was fitted based on an equivalent circuit shown in Figure 6a (inset) [45–47]. The red line represents simulated data with the equivalent circuit, which successfully reproduced the measured Nyquist spectrum. The estimated value of the bulk resistance, R_b, was 6.05×10^3 Ω at 373 K, from which the conductivity of the yellow C_{12}pda-V_{10} hybrids was calculated to be 1.7×10^{-5} S cm^{-1}. This anhydrous conductivity will be owing to the protons which were connected to the V_{10} anions.

Figure 6b shows the temperature dependence of the conductivity for the yellow C_{12}pda-V_{10} hybrids at 313−393 K (40−120 °C). The conductivity at 313 K (40 °C) was 1.1×10^{-8} S cm^{-1}, increased with the increasing temperature, and reached 1.7×10^{-5} S cm^{-1} at 373 K (100 °C). The proton conductivity jumped by three orders of magnitude from that at 313 K to 373 K. However, the conductivity dropped to 9.8×10^{-6} S cm^{-1} at 393 K (120 °C), plausibly due to the removal of water molecules of crystallization by the heating.

The activation energy of the proton conductivity was estimated from the Arrhenius plot as shown in Figure 6c. The value of the slope was obtained by the conductivities except for that at 393 K, where the conduction mechanism would have changed. An obtained value of the activation energy was 1.3 eV (125 kJ/mol), suggesting that the proton conduction mechanism in the yellow C_{12}pda-V_{10} hybrids was more similar to the vehicle mechanism rather than the Grotthuss mechanism [11]. However, the detailed mechanism is unclear and under investigation.

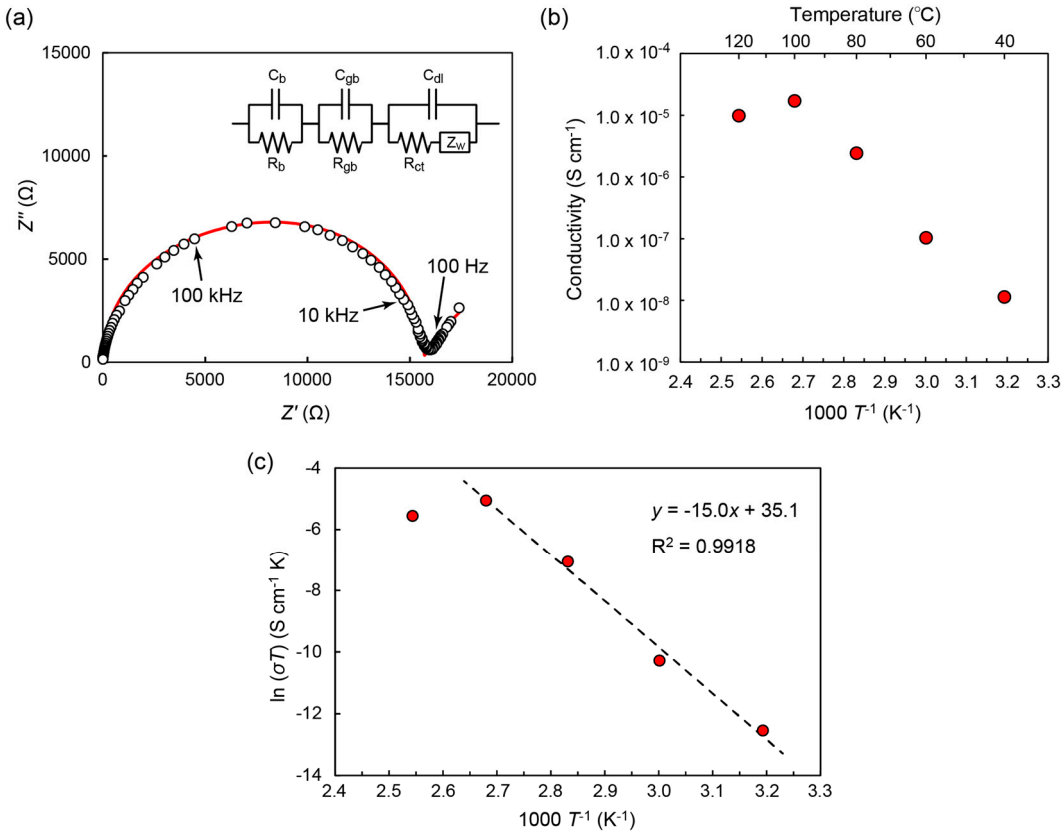

Figure 6. Conductive properties of the yellow C_{12}pda-V_{10} hybrids; (**a**) Nyquist spectrum (open circles) at 373 K and simulated spectrum (red line) based on an equivalent electronic circuit in the figure. The parameters obtained by the fitting: $R_b = 6.05 \times 10^3$ Ω, $R_{gb} = 9.65 \times 10^3$ Ω, $R_{ct} = 1.1 \times 10^3$ Ω, $C_b = 2.5 \times 10^{-8}$ F, $C_{gb} = 5.0 \times 10^{-8}$ F, $C_{dl} = 2.0 \times 10^{-4}$ F, $\sigma = 2.0 \times 10^3$ Ω $s^{-1/2}$ ($Z_w = (1 - j)\sigma/(\omega^{-1/2})$); (**b**) temperature dependence of the conductivity; (**c**) Arrhenius plot of the conductivity. Least-squares fit is shown as a broken line. The fitted results are in the figure.

4. Discussion

Here, the successful crystallization was realized to obtain the single crystals of C_{12}pda-V_{10}. Surfactant-V_{10} hybrid crystals have often been obtained from the synthetic filtrates [36,47,48]. The recrystallization with organic solvents was usually unsuccessful, leading to difficulty in the crystallization of hybrid crystals comprising hydrophobic heterocyclic surfactants. In the case reported here, the different pH values (6.0 and 4.0) were tried to obtain the C_{12}pda-V_{10} hybrids, and suitable single crystals were obtained from the dark green C_{12}pda-V_{10} hybrids obtained at pH 6.0. The dark green C_{12}pda-V_{10} hybrids seemed to contain reduced V_{10} species (Figure 2a), since the dark green color was plausibly derived from the presence of reduced V atoms [16]. The ultraviolet-visible (UV-vis) spectrum of the dark green C_{12}pda-V_{10} hybrids (Figure 7a) suggests the presence of intervalence charge transfers between reduced and fully-oxidized V atoms (ex. V^{IV} and V^{V}), while the yellow C_{12}pda-V_{10} hybrids comprising the fully-oxidized V atoms (BVS values: 5.02–5.07) exhibited no distinct absorption (Figure 7b). However, the detailed oxidation states are unclear. The reduced V_{10} species in the filtrate were gradually oxidized to cause the slow crystallization of the C_{12}pda-V_{10} crystals comprising oxidized and yellow-colored V_{10} species, which had the same molecular and bulk structures as the yellow C_{12}pda-V_{10} hybrids.

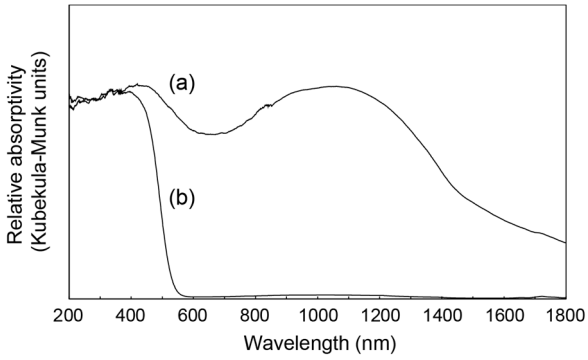

Figure 7. Diffuse reflectance UV-vis spectra of C_{12}pda-V_{10} hybrids: (**a**) dark green C_{12}pda-V_{10} hybrids synthesized at pH 6.0; (**b**) yellow C_{12}pda-V_{10} hybrids synthesized at pH 4.0.

The C_{12}pda-V_{10} crystals contained the diprotonated V_{10} species, and formed a one-dimensional infinite chain structure by the O–H···O hydrogen bonds, which possibly contributed to the emergence of proton-conductivity. In fact, the yellow C_{12}pda-V_{10} hybrids exhibited anhydrous proton conductivity at 313–393 K. The highest value was 1.7×10^{-5} S cm^{-1} at 373 K, but lower than other systems (10^{-3}–10^{-2} S cm^{-1} order for higher conductivity) [7–10]. However, a promising strategy utilizing the proton-containing V_{10} anion and stable heterocyclic surfactants was verified for the emergence of anhydrous proton conductivity. The selection of the surfactants and optimization of the synthetic conditions would pave the way to another class of anhydrous proton conductors.

Supplementary Materials: The following are available online at http://www.mdpi.com/2073-4352/8/2/57/s1, cif file of C_{12}pda-V_{10}.

Acknowledgments: This work was financially supported in part by JSPS KAKENHI Grant Number JP26410245, and Research and Study Program of Tokai University Educational System General Research Organization. X-ray diffraction measurements with synchrotron radiation were performed at the Pohang Accelerator Laboratory (Beamline 2D) supported by Pohang University of Science and Technology (POSTECH).

Author Contributions: Toshiyuki Misawa, Minako Taira and Takeru Ito conceived and designed the experiments; Toshiyuki Misawa and Minako Taira performed the experiments; Toshiyuki Misawa and Takeru Ito analyzed the data; Katsuhiko Fujio contributed materials; Toshiyuki Misawa and Takeru Ito wrote the paper.

Conflicts of Interest: The authors declare no conflict of interest.

References

1. Lehn, J.-M. *Supramolecular Chemistry: Concepts and Perspectives*; VCH: Weinheim, Germany, 1995.
2. Sauvage, J.-P. Transition metal-complexed catenanes and rotaxanes as molecular machine prototypes. *Chem. Commun.* **2005**, *12*, 1507–1510. [CrossRef] [PubMed]
3. Kato, T.; Mizoshita, N.; Kishimoto, K. Functional liquid-crystalline assemblies: Self-organized soft materials. *Angew. Chem. Int. Ed.* **2006**, *45*, 38–68. [CrossRef] [PubMed]
4. Coronado, E.; Gómez-García, C.J. Polyoxometalate-based molecular materials. *Chem. Rev.* **1998**, *98*, 273–296. [CrossRef] [PubMed]
5. Coronado, E.; Giménez-Saiz, C.; Gómez-García, C.J. Recent advances in polyoxometalate-containing molecular conductors. *Coord. Chem. Rev.* **2005**, *249*, 1776–1796. [CrossRef]
6. Steele, B.C.H.; Heinzel, A. Materials for fuel-cell technologies. *Nature* **2001**, *414*, 345–352. [CrossRef] [PubMed]
7. Horike, S.; Umeyama, D.; Kitagawa, S. Ion conductivity and transport by porous coordination polymers and metal-organic frameworks. *Acc. Chem. Res.* **2013**, *46*, 2376–2384. [CrossRef] [PubMed]
8. Yoon, M.; Suh, K.; Natarajan, S.; Kim, K. Proton conduction in metal-organic frameworks and related modularly built porous solids. *Angew. Chem. Int. Ed.* **2013**, *52*, 2688–2700. [CrossRef] [PubMed]
9. Ramaswamy, P.; Wong, N.E.; Shimizu, G.K.H. MOFs as proton conductors–challenges and opportunities. *Chem. Soc. Rev.* **2014**, *43*, 5913–5932. [CrossRef] [PubMed]

10. Tang, Q.; Liu, Y.; Liu, S.; He, D.; Miao, J.; Wang, X.; Yang, G.; Shi, Z.; Zheng, Z. High proton conduction at above 100 °C mediated by hydrogen bonding in a lanthanide metal−organic framework. *J. Am. Chem. Soc.* **2014**, *136*, 12444–12449. [CrossRef] [PubMed]
11. Yamada, T.; Sadakiyo, M.; Kitagawa, H. High proton conductivity of one-dimensional ferrous oxalate dihydrate. *J. Am. Chem. Soc.* **2009**, *131*, 3144–3145. [CrossRef] [PubMed]
12. Colodrero, R.M.P.; Olivera-Pastor, P.; Losilla, E.R.; Hernández-Alonso, D.; Aranda, M.A.G.; Leon-Reina, L.; Rius, J.; Demadis, K.D.; Moreau, B.; Villemin, D.; et al. High proton conductivity in a flexible, cross-linked, ultramicroporous magnesium tetraphosphonate hybrid framework. *Inorg. Chem.* **2012**, *51*, 7689–7698. [CrossRef] [PubMed]
13. Long, D.-L.; Burkholder, E.; Cronin, L. Polyoxometalate clusters, nanostructures and materials: From self assembly to designer materials and devices. *Chem. Soc. Rev.* **2007**, *36*, 105–121. [CrossRef] [PubMed]
14. Nyman, M. Polyoxoniobate chemistry in the 21st century. *Dalton Trans.* **2011**, *40*, 8049–8058. [CrossRef] [PubMed]
15. Proust, A.; Matt, B.; Villanneau, R.; Guillemot, G.; Gouzerh, P.; Izzet, G. Functionalization and post-functionalization: A step towards polyoxometalate-based materials. *Chem. Soc. Rev.* **2012**, *41*, 7605–7622. [CrossRef] [PubMed]
16. Monakhov, K.Y.; Bensch, W.; Kögerler, P. Semimetal-functionalised polyoxovanadates. *Chem. Soc. Rev.* **2015**, *44*, 8443–8483. [CrossRef] [PubMed]
17. Okuhara, T.; Mizuno, N.; Misono, M. Catalytic chemistry of heteropoly compounds. *Adv. Catal.* **1996**, *41*, 113–252.
18. Yamase, T. Photo- and electrochromism of polyoxometalates and related materials. *Chem. Rev.* **1998**, *98*, 307–325. [CrossRef] [PubMed]
19. Sadakane, M.; Steckhan, E. Electrochemical properties of polyoxometalates as electrocatalysts. *Chem. Rev.* **1998**, *98*, 219–237. [CrossRef] [PubMed]
20. Nakamura, O.; Kodama, T.; Ogino, I.; Miyake, Y. High-conductivity solid proton conductors: Dodecamolybdophosphoric acid and dodecatungstophosphoric acid crystals. *Chem. Lett.* **1979**, *8*, 17–18.
21. Honma, I.; Yamada, M. Bio-inspired membranes for advanced polymer electrolyte fuel cells. Anhydrous proton-conducting membrane via molecular self-assembly. *Bull. Chem. Soc. Jpn.* **2007**, *80*, 2110–2123. [CrossRef]
22. Oh, S.-Y.; Yoshida, T.; Kawamura, G.; Muto, H.; Sakai, M.; Matsuda, A. Inorganic-organic composite electrolytes consisting of polybenzimidazole and Cs-substituted heteropoly acids and their application for medium temperature fuel cells. *J. Mater. Chem.* **2010**, *20*, 6359–6366. [CrossRef]
23. Kukino, T.; Kikuchi, R.; Takeguchi, T.; Matsui, T.; Eguchi, K. Proton conductivity and stability of $Cs_2HPW_{12}O_{40}$ electrolyte at intermediate temperatures. *Solid State Ion.* **2005**, *176*, 1845–1848. [CrossRef]
24. Wu, X.; Tong, X.; Wu, Q.; Ding, H.; Yan, W. Reversible phase transformation-type electrolyte based on layered shape polyoxometalate. *J. Mater. Chem. A* **2014**, *2*, 5780–5784. [CrossRef]
25. Tsuboi, M.; Hibino, M.; Mizuno, N.; Uchida, S. Crystalline polyoxometalate (POM)–polyethylene glycol (PEG) composites aimed as non-humidified intermediate-temperature proton conductors. *J. Solid State Chem.* **2016**, *234*, 9–14. [CrossRef]
26. Klaiber, A.; Landsmann, S.; Löffler, T.; Polarz, S. Fourfold action of surfactants with superacid head groups: Polyoxometalate–silicone nanocomposites as promising candidates for proton-conducting materials. *New J. Chem.* **2016**, *40*, 919–922. [CrossRef]
27. Song, Y.-F.; Long, D.-L.; Ritchie, C.; Cronin, L. Nanoscale polyoxometalate-based inorganic/organic hybrids. *Chem. Rec.* **2011**, *11*, 158–171. [CrossRef] [PubMed]
28. Yin, P.; Li, D.; Liu, T. Solution behaviors and self-assembly of polyoxometalates as models of macroions and amphiphilic polyoxometalate-organic hybrids as novel surfactants. *Chem. Soc. Rev.* **2012**, *41*, 7368–7383. [CrossRef] [PubMed]
29. Polarz, S.; Landsmann, S.; Klaiber, A. Hybrid surfactant systems with inorganic constituents. *Angew. Chem. Int. Ed.* **2014**, *53*, 946–954. [CrossRef] [PubMed]
30. Clemente-León, M.; Coronado, E.; Soriano-Portillo, A.; Mingotaud, C.; Dominguez-Vera, J.M. Langmuir-Blodgett films based on inorganic molecular complexes with magnetic or optical properties? *Adv. Colloid Interface Sci.* **2005**, *116*, 193–203. [CrossRef] [PubMed]

31. Nisar, A.; Wang, X. Surfactant-encapsulated polyoxometalate building blocks: Controlled assembly and their catalytic properties. *Dalton Trans.* **2012**, *41*, 9832–9845. [CrossRef] [PubMed]
32. Zhang, T.; Liu, S.; Kurth, D.G.; Faul, C.F.J. Organized nanostructured complexes of polyoxometalates and surfactants that exhibit photoluminescence and electrochromism. *Adv. Funct. Mater.* **2009**, *19*, 642–652. [CrossRef]
33. Qi, W.; Wu, L. Polyoxometalate/polymer hybrid materials: Fabrication and properties. *Polym. Int.* **2009**, *58*, 1217–1225. [CrossRef]
34. Ito, T. Polyoxometalate-surfactant hybrids as building strategy for two-dimensional molecular arrays. *Polyoxometalate Chem.* **2012**, *1*, 6–14.
35. Zhang, G.; Ke, H.; He, T.; Xiao, D.; Chen, Z.; Yang, W.; Yao, J. Synthesis and characterization of new layered polyoxometallates-1,10-decanediamine intercalative nanocomposites. *J. Mater. Res.* **2004**, *19*, 496–500. [CrossRef]
36. Janauer, G.G.; Dobley, A.D.; Zavalij, P.Y.; Whittingham, M.S. Evidence for decavanadate clusters in the lamellar surfactant ion phase. *Chem. Mater.* **1997**, *9*, 647–649. [CrossRef]
37. Spahr, M.E.; Nesper, R. Anhydrous octamolybdate with trimethyl hexadecyl ammonium cations. *Z. Anorg. Allg. Chem.* **2001**, *627*, 2133–2138. [CrossRef]
38. Ito, T. Inorganic-organic hybrid surfactant crystals: Structural aspects and functions. *Crystals* **2016**, *6*, 24. [CrossRef]
39. Ito, T.; Sawada, K.; Yamase, T. Crystal structure of bis(dimethyldioctadecylammonium) hexamolybdate: A molecular model of Langmuir-Blodgett films. *Chem. Lett.* **2003**, *32*, 938–939. [CrossRef]
40. Ito, T.; Yamase, T. Inorganic-organic hybrid layered crystal composed of polyoxomolybdate and surfactant with π electrons. *Chem. Lett.* **2009**, *38*, 370–371. [CrossRef]
41. Ito, T.; Mikurube, K.; Abe, Y.; Koroki, T.; Saito, M.; Iijima, J.; Naruke, H.; Ozeki, T. Hybrid inorganic-organic crystals composed of octamolybdate isomers and pyridinium surfactant. *Chem. Lett.* **2010**, *39*, 1323–1325. [CrossRef]
42. Mikurube, K.; Hasegawa, K.; Naruke, H.; Ito, T. Hybrid layered crystal comprising polyoxometalate and surfactant synthesized from reduced Mo-blue species. *J. Chem.* **2013**, *2013*, 6. [CrossRef]
43. Mikurube, K.; Hasegawa, K.; Matsumoto, T.; Kobayashi, J.; Naruke, H.; Ito, T. Isomerization-induced introduction of metal cations into polyoxomolybdate-surfactant hybrid crystals. *Inorg. Chem. Commun.* **2016**, *73*, 45–48. [CrossRef]
44. Otobe, S.; Fujioka, N.; Hirano, T.; Ishikawa, E.; Naruke, H.; Fujio, K.; Ito, T. Decisive interactions between the heterocyclic moiety and the cluster observed in polyoxometalate-surfactant hybrid crystals. *Int. J. Mol. Sci.* **2015**, *16*, 8505–8516. [CrossRef] [PubMed]
45. Ito, T.; Fujimoto, N.; Uchida, S.; Iijima, J.; Naruke, H.; Mizuno, N. Polyoxotungstate-surfactant layered crystal toward conductive inorganic-organic hybrid. *Crystals* **2012**, *2*, 362–373. [CrossRef]
46. Kobayashi, J.; Kawahara, R.; Uchida, S.; Koguchi, S.; Ito, T. Conductive Hybrid Crystal Composed from Polyoxomolybdate and Deprotonatable Ionic-Liquid Surfactant. *Int. J. Mol. Sci.* **2016**, *17*, 994. [CrossRef] [PubMed]
47. Ito, T.; Taira, M.; Fukumoto, K.; Yamamoto, K.; Naruke, H.; Tomita, K. Polyoxovanadate-surfactant hybrid layered crystal containing one-dimensional hydrogen-bonded cluster chain. *Bull. Chem. Soc. Jpn.* **2012**, *85*, 1222–1224. [CrossRef]
48. Kiyota, Y.; Taira, M.; Otobe, S.; Hanyuda, K.; Naruke, H.; Ito, T. Compositional introduction of lithium ions into conductive polyoxovanadate-surfactant hybrid crystals. *CrystEngComm* **2017**, *19*, 3037–3043. [CrossRef]
49. Nyman, M.; Ingersoll, D.; Singh, S.; Bonhomme, F.; Alam, T.M.; Brinker, C.J.; Rodriguez, M.A. Comparative study of inorganic cluster-surfactant arrays. *Chem. Mater.* **2005**, *17*, 2885–2895. [CrossRef]
50. Nyman, M.; Rodriguez, M.A.; Anderson, T.M.; Ingersoll, D. Two structures toward understanding evolution from surfactant-polyoxometalate lamellae to surfactant-encapsulated polyoxometalates. *Cryst. Growth Des.* **2009**, *9*, 3590–3597. [CrossRef]
51. Du, H.-J.; Mi, L.-W.; Yue, Z.-C.; Niu, Y.-Y.; Hou, H.-W. Templated fabrication, isomer recognition of series of 1,10-(alkane-1, ω-diyl)-bis(3-methylimidazolium)-induced polyoxometalates (ω = 1–11). *Inorg. Chim. Acta* **2014**, *409*, 418–426. [CrossRef]

52. Yue, Z.-C.; Du, H.-J.; Li, L.; Zhang, W.-L.; Niu, Y.-Y.; Hou, H.-W. Construction and isomer recognition of polyoxometalates functionalized by 1,2-dimethylimidazole alkane templates. *Inorg. Chim. Acta* **2014**, *410*, 136–143. [CrossRef]
53. Jiang, Y.; Liu, S.; Li, S.; Miao, J.; Zhang, J.; Wu, L. Anisotropic ionic liquids built from nonmesogenic cation surfactants and Keggin-type polyoxoanions. *Chem. Commun.* **2011**, *47*, 10287–10289. [CrossRef] [PubMed]
54. Yin, P.; Wu, P.; Xiao, Z.; Li, D.; Bitterlich, E.; Zhang, J.; Cheng, P.; Vezenov, D.V.; Liu, T.; Wei, Y. A double-tailed fluorescent surfactant with a hexavanadate cluster as the head group. *Angew. Chem. Int. Ed.* **2011**, *50*, 2521–2525. [CrossRef] [PubMed]
55. Zhu, L.; Chen, K.; Hao, J.; Wei, Z.; Zhang, H.; Yin, P.; Wei, Y. Synthesis and crystallization behavior of surfactants with hexamolybdate as the polar headgroup. *Inorg. Chem.* **2015**, *54*, 6075–6077. [CrossRef] [PubMed]
56. Day, V.W.; Klemperer, W.G.; Maltbie, D.J. Where are the protons in $H_3V_{10}O_{28}^{3-}$? *J. Am. Chem. Soc.* **1987**, *109*, 2991–3002. [CrossRef]
57. Ferreira da Silva, J.L.; Minas da Piedade, M.F.; Duarte, M.T. Decavanadates: A building-block for supramolecular assemblies. *Inorg. Chim. Acta* **2003**, *356*, 222–242. [CrossRef]
58. Nakamura, S.; Ozeki, T. Hydrogen-bonded aggregates of protonated decavanadate anions in their tetraalkylammonium salts. *J. Chem. Soc. Dalton Trans.* **2001**, 472–480. [CrossRef]
59. Nakamura, S.; Ozeki, T. Guest driven rearrangements of protonation and hydrogen bonding in decavanadate anions as their tetraalkylammonium salts. *Dalton Trans.* **2008**, 6135–6140. [CrossRef] [PubMed]
60. Kojima, T.; Antonio, M.R.; Ozeki, T. Solvent-driven association and dissociation of the hydrogen-bonded protonated decavanadates. *J. Am. Chem. Soc.* **2011**, *133*, 7248–7251. [CrossRef] [PubMed]
61. Román, P.; Aranzabe, A.; Luque, A.; Gutiérrez-Zorrilla, J.M.; Martinez-Ripoll, M. Effects of protonation in decavanadates: Crystal structure of tetrakis(*n*-hexylammonium) dihydrogendecavanadate(V). *J. Chem. Soc. Danton Trans.* **1995**, 2225–2231. [CrossRef]
62. Fujio, K.; Ikeda, S. Size of spherical micelles of dodecylpyridinium bromide in aqueous NaBr solutions. *Langmuir* **1991**, *7*, 2899–2903. [CrossRef]
63. Otwinowski, Z.; Minor, W. Processing of X-ray diffraction data collected in oscillation mode. *Methods Enzymol.* **1997**, *276*, 307–326. [PubMed]
64. Sheldrick, G.M. SHELXT—Integrated space-group and crystal structure determination. *Acta Crystallogr. Sect. A* **2015**, *71*, 3–8. [CrossRef] [PubMed]
65. Sheldrick, G.M. A short history of SHELX. *Acta Crystallogr. Sect. A* **2008**, *64*, 112–122. [CrossRef] [PubMed]
66. *CrystalStructure 4.2*; Rigaku Corporation: Tokyo, Japan, 2017.
67. Cruywagen, J.J. Protonation, oligomerization, and condensation reactions of vanadate(V), molybdate(VI), and tungstate(VI). *Adv. Inorg. Chem.* **1999**, *49*, 127–182.
68. Brown, I.D.; Altermatt, D. Bond-valence parameters obtained from a systematic analysis of the inorganic crystal structure database. *Acta Crystallogr. Sect. B* **1985**, *41*, 244–247. [CrossRef]
69. Desiraju, G.R.; Steiner, T. The Weak Hydrogen Bond. In *Structural Chemistry and Biology*; Oxford University Press: New York, NY, USA, 1999; pp. 12–16.